



Contents lists available at ScienceDirect

Quaternary International

journal homepage: www.elsevier.com/locate/quaint

Direct push sensing in wetland (geo)archaeology: High-resolution reconstruction of buried canal structures (*Fossa Carolina*, Germany)

Jörg Hausmann ^{a,1}, Christoph Zielhofer ^{b,*}, Lukas Werther ^c, Stefanie Berg-Hobohm ^d, Peter Dietrich ^{a,e}, Robert Heymann ^b, Ulrike Werban ^a

^a UFZ – Helmholtz Centre for Environmental Research, Department Monitoring and Exploration Technologies, Leipzig, Germany

^b Leipzig University, Chair of Physical Geography, Leipzig, Germany

^c Friedrich Schiller University, Seminar of the Archaeology of Prehistory to the Early Middle Ages, Jena, Germany

^d BLfD – Bavarian State Department for Cultural Heritage, Munich, Germany

^e Eberhard Karls University, Centre of Applied Geosciences, Tübingen, Germany

ARTICLE INFO

Article history:

Received 28 June 2016

Received in revised form

20 January 2017

Accepted 8 February 2017

Available online xxx

Keywords:

Wetland geoarchaeology

Direct push sensing

Conductivity logging

Color logging

Parameter prediction

Fossa Carolina

ABSTRACT

(Geo)archaeological trenching techniques in floodplain and wetland environments are challenging due to the impact of groundwater inflow and highly unstable trench edges. Alternatively, classical driving core techniques often correspond with the contraction of organic layers and bias in height accuracies. Here, we present the application of direct push sensing techniques for minimal-invasive (geo)archaeological surveys in zones affected by a high groundwater table, especially when high-resolution parameterization of buried (geo)archaeological structures is required.

Two of these direct push applications are electrical conductivity logging and the measurement of colorimetric proxies in unconsolidated sediments. The tools provide multi-proxy information about layer structure, texture, and organic parameters. The high sensing speed allows recording a large data set with high vertical and lateral resolution. In this study we exemplarily provide results of a buried canal structure within a valley in SW Germany. We present a high-resolution cross-section from a zone of high groundwater table. The canal is part of Charlemagne's summit canal (*Fossa Carolina*), an Early Medieval hydro-engineering project bridging the Central European Watershed.

We compare the direct push sensing data with driving core samples and discuss prediction and generation options of parameter transfer from multiple one-dimensional logs to a two-dimensional canal cross-section of high-resolution. In this context, we use *in situ*-obtained colorimetric data and electrical conductivity as proxies for (geo)archaeological site characterization. We model organic fills of the canal by direct push logs and robust sediment data. Given the cost and time effectiveness of such tools, (geo) archaeological site information of high-depth accuracy was grown rapidly, compared to less densely performed drillings that require an additional high effort in laboratory analyses.

The Carolingian excavation depth is 6 m below current surface. There is evidence for multiple organic layers in the trench fills, which reveal aquatic to semi-terrestrial stillwater deposition and, therefore, evidence of multiple Carolingian and post-Carolingian ponds. We have evidence for a conceptual width of the deep-buried artificial water course of at least 3–4 m. This allows a passage of Carolingian cargo scows with a payload of several tons in this central zone of the canal.

© 2017 The Authors. Published by Elsevier Ltd. This is an open access article under the CC BY-NC-ND license (<http://creativecommons.org/licenses/by-nc-nd/4.0/>).

1. Introduction

Wetland margins are important zones in (geo)archaeological research (Brown, 1997). Those locations are valuable (geo)archaeological archives, since high groundwater level in wetland and floodplain environments ordinarily provides excellent preservation conditions for palaeoecological and geomorphological proxy-parameters, archaeological remnants, artefacts, and organic

* Corresponding author.

E-mail address: zielhofer@uni-leipzig.de (C. Zielhofer).

¹ Present address: Basalt-Aktion-Gesellschaft, Department URL, Wiedemar, Germany.

compounds (Plets et al., 2007; Menotti and O'Sullivan, 2013). However, wetlands are characterized by difficult exploration conditions that require complicate and costly excavation techniques due to the impact of groundwater inflow (Doran, 2013) and highly unstable trench edges (Werther and Feiner, 2014). Furthermore, alternatively used classical driving core techniques—common tools in wetland (geo)archaeological surveys—often suffer from high compaction rates of organic layers and, thus, shows a bias in depth accuracies (Leithold et al., 2012, 2014). Hence, there is a demand on alternative tools for the conduction of (geo)archaeological surveys in wetlands.

Direct push methods are getting increasingly accepted in the water, contaminant, and geotechnical sectors (McCall et al., 2005; Dietrich and Leven, 2006; Leven et al., 2010; Zschornack and Leven-Pfister, 2012a). Direct push electrical conductivity logging (Christy et al., 1994; Schulmeister et al., 2003; Zschornack and Leven-Pfister, 2012b) and cone penetration testing (Lunne et al., 1997; Brouwer, 2007) are probably the most common applications. The application of such techniques, however, for palaeoenvironmental and (geo)archaeological investigations just recently started to develop. Koster (2015), Missiaen et al. (2015), and Vos et al. (2015) use cone penetration testing for mapping buried surfaces and walking horizons at archaeological sites. Fischer et al. (2016) coupled direct push electrical conductivity logging to near surface electrical resistivity tomography improving (geo)archaeological site interpretation. Dalan et al. (2011) and Matney et al. (2014) provide examples using optical direct push probes for archaeological prospection.

In soil science, color logging is used for recording soil parameterization and stratigraphic boundaries (Hartemink and Minasny, 2014). Here, soil color is a useful proxy for the content of organic matter (Wills et al., 2007; Eckmeier et al., 2013). Recently, Hausmann (2014) and Hausmann et al. (2016) recognized real-time *in situ*-obtained colorimetric data as a promising direct push proxy

for site characterization and also demonstrated its site-specific relation to cone penetration testing and direct push electrical conductivity logging. Regarding color logging, (geo)archaeological sites in wetlands are a challenging investigation object, while the preservation conditions in this environment provide high colorimetric contrasts (Gerlach et al., 2012) due to a high variability in organic and clastic layering with changing redox conditions.

The main goal of this study is to access the potential of *in situ* colorimetric proxy sensing for (geo)archaeological applications in wetlands. We perform a combination of direct push methods for sampling and sensing. Thus, we focus on the application of direct push color sensing accompanied by direct push electrical conductivity sensing and sedimentological analyses of driving core samples. Additionally, we present and discuss options for parameter transfer from multiple one-dimensional logs towards a two-dimensional high-resolution cross-section.

We focus here on a prominent German study site in wetland (geo)archaeology: Charlemagne's *Fossa Carolina*, an Early Medieval summit canal project (Fig. 1) bridging the Central European Watershed in 793 AD (Ettel et al., 2014; Zielhofer et al., 2014; Werther et al., 2015). Here, we will expand the (geo)archaeological data density along a canal cross-section in the central zone of the building, where regular archaeological excavations are not possible. We aim to reconstruct the canal structure – including the refilling process – and to gain information about the Carolingian construction stage and the potential use of the structure in Carolingian and post-Carolingian times.

2. Regional setting and site description

The Central European Watershed divides the Rhine-Main and Danube catchments (Fig. 1a). In the Early Medieval period, when ships were important means of transportation, Charlemagne decided to link both catchments by the construction of a canal

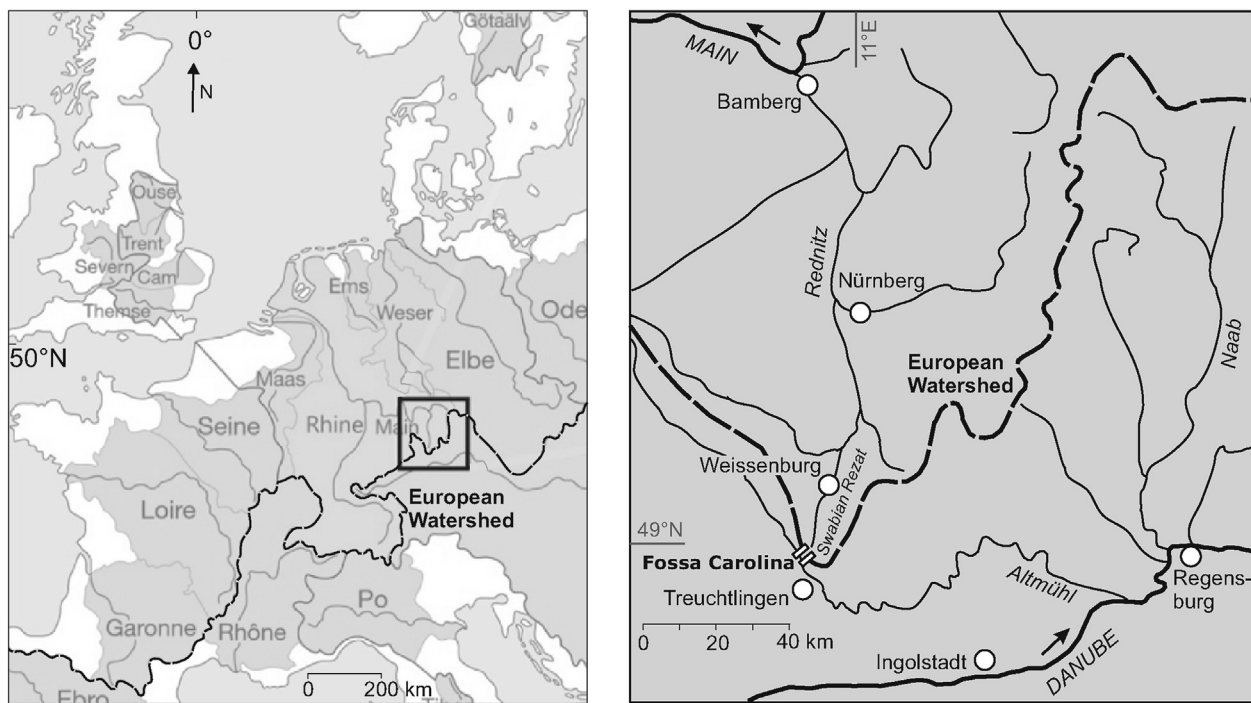


Fig. 1. Regional setting of the *Fossa Carolina* (Zielhofer et al., 2014): a) The Central European Watershed divides the Rhine-Main and the Danube catchments. b) The Early Medieval *Fossa Carolina* links the Swabian Rezat and the Altmühl Rivers.

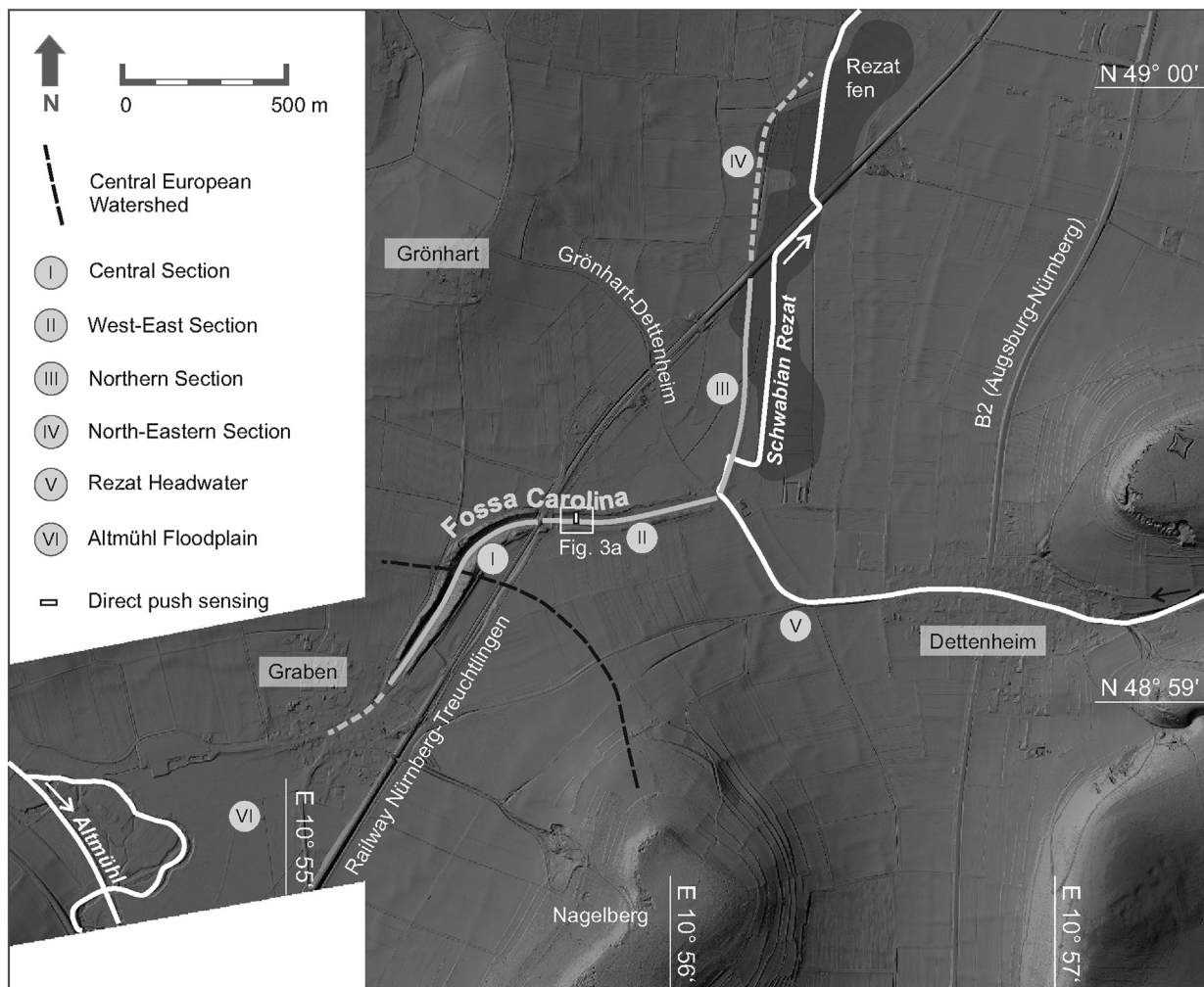


Fig. 2. The course of the *Fossa Carolina* and the subdivision in six sections (Zielhofer et al., 2014): I) Central Section, II) West-East Section, III) Northern Section, IV) North-Eastern Section, V) Rezat Headwater, and VI) Altmühl Floodplain. Raw data source: LIDAR data are cordially provided by Bavarian Land Surveying Office for illustrative purposes.

connecting the Swabian Rezat and Altmühl Rivers (Fig. 1b). This artificial waterway would provide a continuous inland navigation route from the North Sea to the Black Sea. The shortcut is known as *Fossa Carolina* and represents one of the most important Early Medieval engineering achievements in Europe. The potential Carolingian use and functioning of the canal is currently under debate (Zielhofer et al., 2014; Werther et al., 2015; Kirchner et al., this issue).

The *Fossa Carolina* is located in the Southern Franconian Jura. It is surrounded by Upper Jurassic (Malm) carbonate rocks and Middle Jurassic Aalenian (Dogger Beta) sandstones (Schmidt-Kaler, 1976, 1993; Zielhofer et al., 2014). The Swabian Rezat River is a small tributary of the Rhine-Main river system whereas the Upper Altmühl River is a tributary of the Danube River (Fig. 1b). Swabian Rezat River and Upper Altmühl River flow through undulating Middle Jurassic Aalenian (Dogger Alpha) and Lower Jurassic (Lias) foothills. The canal is not directly situated on the Middle Jurassic Aalenian clayey sediments, but rather on Quaternary fills consisting of predominantly fluvial sands. The location of the *Fossa Carolina* is closely associated with the position of the Altmühl and Swabian Rezat Rivers (Figs. 1b and 2). The modern mean water level of the Altmühl at its supposed confluence with the *Fossa Carolina* is 408.3 m a.s.l. (Zielhofer et al., 2014).

The *Fossa Carolina* can be divided in six (geo)archaeological sections. Within the Central Section and the West-East Section impressive banks up to 6.5 m high are still visible (Fig. 2) (Schwarz, 1962). A synthesized longitudinal profile of the trench fills from previous (geo)archaeological drillings reveal evidence for a summit canal as the final hydro-engineering concept (Koch et al., 1993; Koch and Leininger, 1993; Leitholdt et al., 2014; Zielhofer et al., 2014).

The longitudinal canal profile gave proof that the artificial and labor intensive dislocation of the natural watershed allows the opportunity to supply the summit of the Carolingian canal with Rezat spring water (Zielhofer et al., 2014) that corresponds hydrogeologically with the shallow karst aquifers of the Southern Franconian Jura (Zielhofer, 2004, 2009). Hence, Charlemagne's canal features an extraordinarily advanced construction level for a navigable waterway. This is confirmed by an archaeological excavation within the Northern Section of the canal that resulted in the recovery of multiple Carolingian oak planks in summer 2013. The timber was used for bank stabilization and dendrochronological analyses (Werther and Feiner, 2014; Werther et al., 2015) confirm the date of construction in autumn 793 AD (Hack, 2014).

Regarding the southern continuation of the canal, previous (geo) archaeological and geophysical surveys within the zone of the

Altmühl floodplain (Fig. 2) does not provide any indication yet for an existing connection of the canal with the Altmühl River (Kirchner et al. this issue). This is in accordance with written sources. Available historical data imply that the canal was never completed (Hack, 2014).

Previous (geo)archaeological findings from a driving core cross-section within the West-East-Section of the canal (Figs. 3b and 4) provide evidence for a buried canal structure. The organic fills indicate the onset of aquatic and semi-terrestrial conditions in the Carolingian period and reveal multiple ponding phases until modern times (Zielhofer et al., 2014). However, due to the high groundwater level, an archaeological excavation is time-consuming and expensive in this zone of the canal. Furthermore, it would ultimately destroy a significant part of the site. Therefore, the detailed architecture of the Carolingian trench, a probable timber-use, the high-resolution stratigraphy of the canal fills, and the intercalation of the canal fills with the adjacent colluvial refills is not known yet.

3. Material and methods

3.1. General characteristics of direct push methods

Direct push (DP) technologies are defined as part of a growing family of tools used for performing subsurface investigations by driving, pushing, and/or vibrating small-diameter, hollow steel rods into the ground (EPA, 1997). They are most applicable in unconsolidated sediments that are typically less than 30 m below the surface (EPA, 2005). Several attachable tools and probes are available for minimally invasive logging of geophysical, geotechnical, hydrological and geochemical data (Dietrich and Leven, 2006; Zschornack and Leven-Pfister, 2012a). Thus, considering small-scale variability, continuous *in situ* measurements of subsurface properties provide high-resolution vertical and reproducible data logs up to a cm-scale (Leven et al., 2011; Zschornack and Leven-Pfister, 2012a). These data provide many advantages in

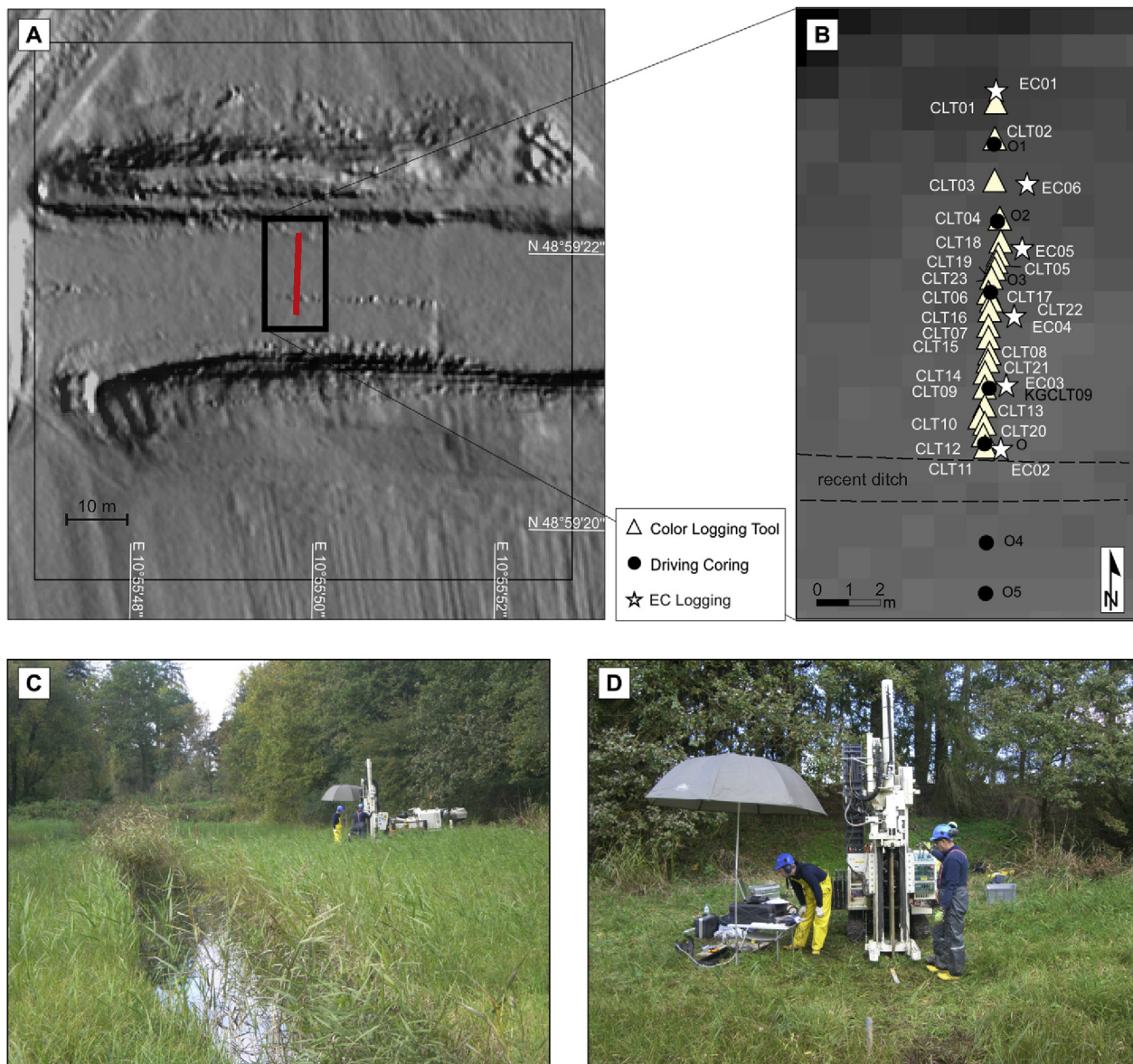


Fig. 3. Fossa Carolina West-East Section local setting: a) Locality of the canal cross-section (red line, this study). b) Direct push sensing and driving coring positions. c) Direct push sensing (view to the West). d) Direct push sensing (view to the North). (For interpretation of the references to colour in this figure legend, the reader is referred to the web version of this article.)

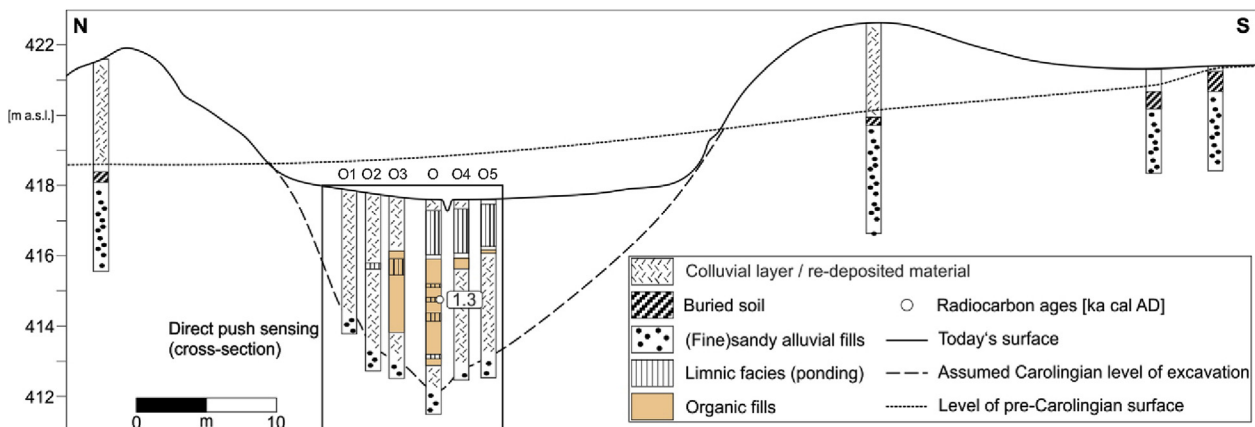


Fig. 4. Cross-section of the *Fossa Carolina* West-East Section (Zielhofer et al., 2014) with the indicated zone of direct push sensing (this study).

comparison to common drilling methods, due to avoidance of compaction or contamination effects during soil removal. In this study, in autumn 2014 direct push sensing of depth-accurate *in situ* parameter in a cm-resolution was performed by self-propelled carrier vehicle (Geoprobe) with attached direct push electrical conductivity and color probes. All starting points were levelled by a depth-accurate Topcon DGPS system in cm-resolution.

3.2. Direct push electrical conductivity logging

Spatial variability of electrical conductivity σ and its reciprocal, electrical resistivity ρ , reveal numerous information of sediment matrix properties like water content, grain size, or salinity (Hoffmann and Dietrich, 2004). On this note, direct-push driven electrical conductivity logging provides *in situ* high-resolution records of sub-surface electrical properties in multiple cm-scale (Butler et al., 1999; Hausmann et al., 2013; Hausmann, 2014). This method is a robust tool that can distinguish between different unconsolidated sediment types especially in the saturated zone (Chouker, 1971; Schulmeister et al., 2003). In this study, we use a Geoprobe SC-500 probe for recording electrical conductivity (Christy et al., 1994). We set the probe's four equally spaced electrodes in a Wenner array. The data are constantly logged while pushing the probe downwards (Zschornack and Leven-Pfister, 2012b).

Similar to the studies of Butler et al. (1999), Hausmann et al. (2013), and Hausmann (2014), we conduct direct push electrical conductivity logs in a multiple cm-scale. However, the obtained depth-relevant value is the result of an integral that represents all lithological information defined by the electrode spacing. Thus, resolution is limited due to the technical setup of the probe, containing four electrodes in 2.5-cm spacing, respectively 7.5 cm in total (Christy et al., 1994). Consequently, direct push electrical conductivity logs document clear lithological changes, whereas the detection of very thin intercalated layers at mm-to cm-scale is somewhat limited.

3.3. Direct push color logging

For *in situ*-sensing of visible colors, we applied the soil optical color screening tool (SCOST™), Dakota technologies (Dalan et al., 2011; Hausmann, 2014; Hausmann et al., 2016). The color logging tool (CLT) is made of a tri-stimulus colorimeter system, which consists of a light source, a photo-sensitive detector and a hollow soil penetrometer. The source induces white light, which is conducted via optical fibers to the probe into the sub-surface. The

reflected light is recorded under standardized observation conditions (10°-observer, reference to D₆₅ white point). The depth resolution depends on the probing velocity and the pre-set measurement interval (Hausmann et al., 2016). In this study, we achieved an average probing velocity of approx. 1 cm/s resulting in an average depth resolution of 5 mm. As a result, post-processing of colorimetric data in combination with depth information provides a high-resolution vertical color record in cm-scale.

For rapid visualization of the color logs, RGB raster images are computed. Following Hausmann et al. (2016), the raw data were processed for subsequent analyses to CIEL* a^* b^* color space (Wyszecki and Stiles, 1982; Ohta and Robertson, 2005). Thus, we achieve physically independent colorimetric proxy data expressed as luminosity (L^*), scaling from 0 (black) to 100 (white), and chromatographic coordinates a^* (red-green ratio) and b^* (blue-yellow ratio). For the reduction of high natural color variability, we applied a wavelet filter (Hausmann et al., 2016).

3.4. Recovery of driving cores

Sediments were recovered by a hand-held Cobra Pro (Atlas Copco) driving core drilling system and 60-mm diameter open corer. During driving, no rotation of sediment is involved, since the tool is only pushed into the ground. The achieved segments of each 1-m lengths were accessed on site towards sediment features according to AG Boden (2005). The recovered segments were documented, photographed, and sampled in a 5–10 cm resolution for subsequent laboratory analysis. Additionally, we took distinct colorimetric measurements on the sediment samples with the SCOST™ color probe right after sampling the core.

3.5. Sedimentological analyses

We determined grain size median (D₅₀) and distributions of each sediment layer to obtain information about the texture and the corresponding deposition process. This method is applicable to samples with a content of organic matter less than 5% (Zielhofer et al., 2014). Bulk samples (10 g) were left in 50 ml 35%-hydrogen peroxide (H₂O₂) overnight, and heated to remove organic matter during the next day. Afterwards, the samples were dispersed using 10 ml 0.4 N sodium pyrophosphate solution (Na₄P₂O₇) and ultrasonic treatment for 45 min. Grain size analysis of the sand fraction was carried out by means of the dry-sieving technique (2000–630 µm: coarse sand, 630–200 µm: medium sand, 200–125 µm: fine sand, 125–63 µm: finest sand). Coarse silt (63–20 µm), medium silt (20–6.3 µm), fine silt (6.3–2.0 µm), coarse

clay ($2.0\text{--}0.6 \mu\text{m}$), medium clay ($0.6\text{--}0.2 \mu\text{m}$) and fine clay ($<0.2 \mu\text{m}$) were measured by X-ray granulometry (XRG) using a SediGraph III 5120 (Micromeritics).

For calculating the content of organic matter (OM), we measured the content of total carbon (TC) by using a CNS analyser vario EL cube (Elementar), and determined the content of inorganic carbon (TIC) by calcimeter measurements (Scheibler method, Eijkelkamp). Resulting values of organic carbon (TOC) were multiplied by 1.72 in order to obtain contents of organic matter (OM). In addition, total nitrogen (TN) and total sulfur (TS) were measured and C/N ratio was computed.

4. Results and interpretation

4.1. Canal cross-section: sedimentological features

We recovered an additional driving core (KGCLT09, Figs. 3b and 5) from the previous canal cross-section (Fig. 4). We separate the core in three major sub-sections (Fig. 6):

- (1) The *lower sub-section* features a clastic stratigraphy from 410.63 to 412.23 m a.s.l. The lowermost part of the sub-section reveals fluvial sands of gray-yellowish color with D50 values spanning $205\text{--}594 \mu\text{m}$ (medium sand). Above 411.85 m a.s.l., we observe a change in redox state towards dominant grayish colors representing reductive conditions. Organic contents also rise from 0.1 to 3%. The grain size shows a clear fining-up towards a grayish clay layer at 412.23 m a.s.l.
- (2) The *middle sub-section* (412.23–415.97 m a.s.l.) generally reveals organic layers with clastic intercalations. From 412.23 to 415.42 m a.s.l. the organic content clearly increases, reaching a maximum (>40%) at 414.33 m a.s.l. The peat and intercalated sapropel layers reveal dark gray to blackish colors. We detect sapropel layers at 412.83 to 412.93, 413.83 to 413.93, 414.92 to 415.02, and 415.15–415.16 m a.s.l. Between 415.42 and 415.53 m a.s.l. a sandy to loamy clastic layer separates the organic sediments. The middle sub-section ends with organic-rich, grayish to black fen deposits from 415.53 to 415.97 m a.s.l. We found a larger piece of wood at 412.62 m a.s.l.

- (3) The *upper sub-section* (415.97–417.63 m a.s.l.) reveals predominantly clastic layers with varying grain sizes. Layers between 415.97 and 416.16 m a.s.l. reveal grayish medium sands ($D_{50} = 300 \mu\text{m}$). Layers from 416.13 to 417.01 m a.s.l. feature a fining-up sequence towards silty and clayey deposits ($D_{50} = 2\text{--}10 \mu\text{m}$) with high color diversity, spanning brownish-grayish-ocher tones. Subsequent sandy layers from 417.01 to 417.18 m a.s.l. show indications for oxidation. Uppermost layers composed of loamy sediments with median grain sizes (D_{50}) between 16 and $25 \mu\text{m}$. The organic content slightly increases again and the colors indicate hydromorphic redox conditions.

4.2. Canal cross-section: electrical conductivity logging and texture

The correlation between texture and direct push electric conductivity data is also visible in the direct comparison of EC03 log (Figs. 6f and 7) with KGCLT09 core stratigraphy (Fig. 6a and b). The relative low electric conductivities σ of approx. 20 mS/m in the *lower sub-section* correspond with medium sands. Since the fluvial sands do not shift significantly in grain size, electrical conductivities also do not show obvious oscillations.

No grain size data are available for the organic rich-layers of the *middle sub-section* of the core (Fig. 6b). However, the organic-rich layers reveal relatively constant electrical conductivities approx. 40 mS/m that might indicate a homogeneous texture of the organic-rich sub-section.

The *upper sub-section* features electrical conductivities from 20 to 68 mS/m with lower values at the bottom and at the top (Fig. 6f). The low values correspond with low clay contents (Fig. 6b).

Observed *core losses* in the driving core record (notated ‘n/a’) most likely refer to compaction effects during coring. Especially, we observe high compaction rates within the organic fills of the middle sub-section. As we have to consider a bias in height accuracy within the driving core record (Fig. 6a) we conduct a height correction. Direct push electrical conductivity logs and color logs represent a record with high depth-accuracy (Fig. 6f). Hence, we use these records as a standard for depth levels. Additionally, we used the levels of the penetrated drilling heads of the individual 1-m long driving cores as fixed marks with exact depth accuracy. Subsequently,

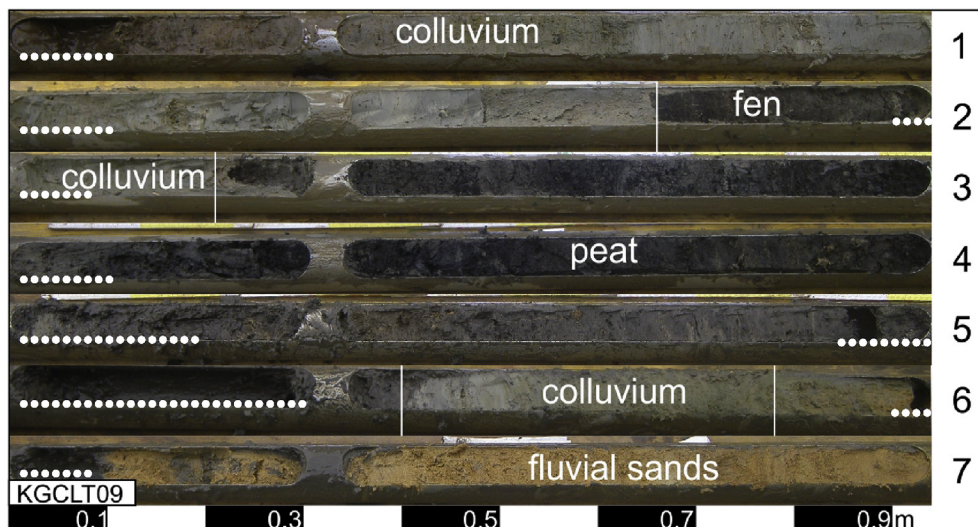


Fig. 5. Photographs of driving core KGCLT09 from the *Fossa Carolina* West-East Section. Meters represent depth from surface. White dotted lines indicate zones of missing or disturbed strata.

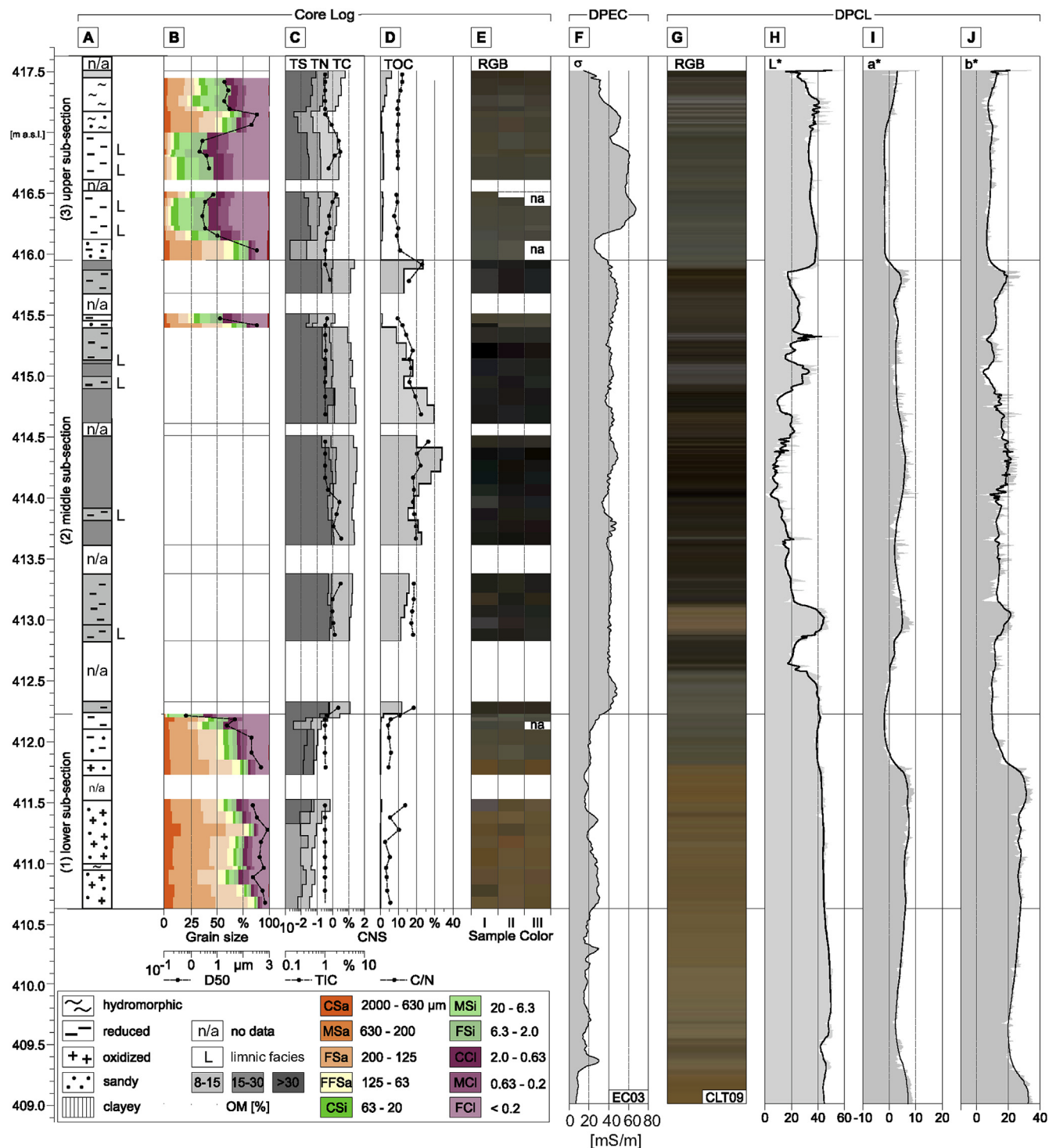


Fig. 6. a) KGCLT09 driving core stratigraphy with organic matter (OM). b) Cumulative grain size and median diameter D50. c) Total sulfur (TS), total nitrogen (TN), total carbon (TC), total inorganic carbon (TIC). d) total organic carbon (TOC), TOC/TN ratio. e) Distinct and three-times repeated **RGB** color records of individual sediment samples. f) Direct push electrical conductivity σ (EC03). g) Direct push color logging (CLT09)**RGB**. h) Luminosity L^* . i) Chromatographic coordinates red-green ratio a^* and j) blue-yellow ratio b^* from CIEL a^* b^* color space. (For interpretation of the references to colour in this figure legend, the reader is referred to the web version of this article.)

stretching of the core stratigraphy was applied only within the range of the 1-m long driving cores. This leads to a virtual extension of the recovered sediment layers in the vertical domain. As a result, Fig. 7 depicts correlations of the sand (2000–63 µm) and clay fractions (2.0–0.2 µm) from core KGCLT09 after height correction with measured electrical conductivities.

Fig. 8b shows a compilation of all direct push electrical conductivity logs for the entire canal cross-section. The electrical conductivity data reveal a total range from 2 to 68 mS/m. Between 409.90 and 411.70 m a.s.l., in the lower northern part of the cross-section we detect a noticeable zone with electric conductivities above 30 mS/m (EC06, EC05, EC04, EC02) that are not ubiquitous at

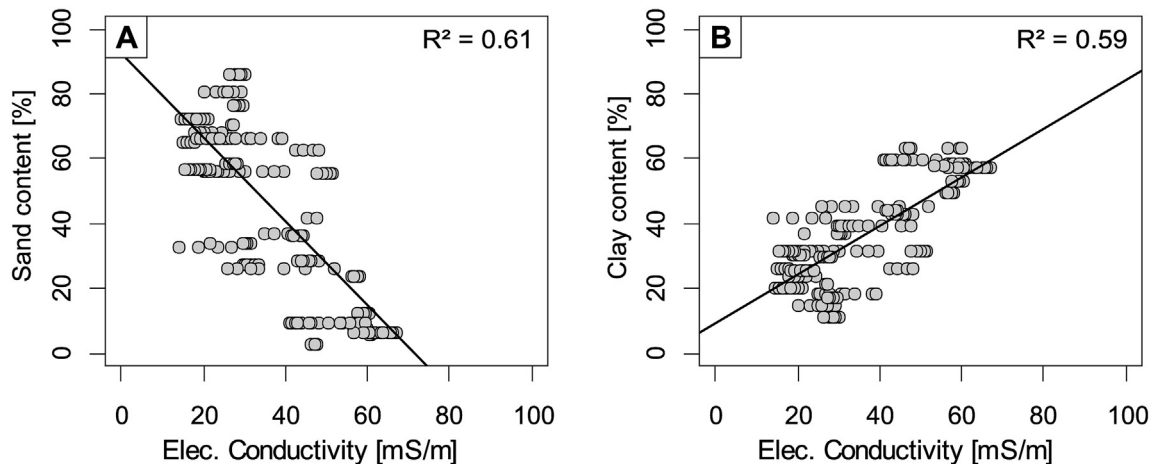


Fig. 7. Linear correlation between direct push electrical conductivity (DPEC) σ of log EC03 and texture from KGCLT09 core: a) Sand fraction (2000–63 μm) versus σ (mS/m). b) Clay fraction (2.0–0.2 μm) versus σ ($\mu\text{S}/\text{cm}$). Due to the higher resolution of the EC logs, multiple EC logs correspond with single grain size value.

this level: EC03 log does not feature electric conductivities of more than 30 mS/m, indicating a change in sediment facies within this level. Fig. 9a depicts a 2D visualization for the conducted electrical conductivity logs. We applied block kriging algorithm (size 0.5×0.5 m) constraint by geospatial correlation (variogram). The 2D visualization also shows the high electrical conductivity values in the lower northern zone of the cross-section.

4.3. Canal cross-section: colorimetric proxies and stratigraphical features

For a better validation of the direct push-derived colorimetric logs, we added on site colorimetric measurements of recovered sediment samples from driving cores as an intermediate step. Fig. 6e shows the colorimetric data from KGCLT09 core, taken directly after the sampling procedure in the field. We conducted repeated measurements, resulting in three measurements per soil sample. The computed **RGB** values can be directly coupled with documented sediment features.

The correlation between stratigraphical features and direct push colorimetric proxies is visible in the direct comparison of color logs (Fig. 6g to j) with the KGCLT09 core stratigraphy (Fig. 6a) and texture (Fig. 6b). The lower sub-section features high luminosity ($L^* > 40$), positive red values ($a^* > 0$) and enhanced yellow values ($b^* > 20$), which corresponds with oxidized fluvial sands. From 411.82 to 412.60 m a.s.l., the clastic layers feature reductive conditions. Here, the colorimetric composition turns to green ($a^* < 0$) with less intense yellow ($b^* < 20$).

The middle sub-section is characterized by the dominance of organic layers. The colorimetric proxies feature noticeable changes. Luminosity L^* is very low (5–20) reaching almost black. Red (a^*) and yellow (b^*) values are positive. We deduce a pale-colored layer within the middle sub-section (approx. 412.85–413.11 m a.s.l.), which corresponds with a large wood remnant. High-frequency variability of the colorimetric data in the middle sub-section features a fine horizontal bedding of the alternating peat and sapropel layers.

The upper sub-section features predominantly reduced clastic layers. The gray coloring is indicated by a medium luminosity (L^* approx. 40). The uppermost part of the section shows a shift towards a lower luminosity and enhanced red values ($a^* > 0$), indicating a semi-terrestrial horizon.

Fig. 8c shows a compilation of all direct push **RGB** logs for the entire canal cross-section. We achieved an extremely high lateral

resolution (low spacing) of the starting points for direct push colorimetric logs up to approx. 0.25 m distance, which was close to exceed technical realization. Totally, we conducted 23 vertical colorimetric logs. Generally, the colors show high contrasts. Grayish-brown colors represent organic canal fills, yellowish-red colors indicate oxidized clastic sediments and pale gray colors feature oxygen-reduced layers. Due to the high lateral resolution of the color logs and the high depth-accuracy, a stratigraphical coupling of the single **RGB** logs is possible. As a result, we receive a high-resolution **RGB** composite image of the buried canal structure.

Considering the sedimentological features from KGCLT09 core, the **RGB** logs (Fig. 8c) indicate changes in redox conditions, texture and organic contents (Fig. 8a) that corresponds with varying phases of geomorphological activity and stagnancy. Active phases of canal aggradation represent colluvial deposition at the canal edges and clastic alluvial fills in the central zone. Stagnation phases represent geomorphological stability with ponding and the development of semi-terrestrial organic layers. Between 412.5 and 416.5 m a.s.l., the **RGB** logs reveal alternating grayish-brown and almost black colors, which correspond to peat and sapropel layers. This zone indicates the aquatic to semi-terrestrial zone of the canal with potential former ponds. The organic fills show a lateral extension of approx. 5 m. The direct push **RGB** logs do not cover the whole extent of the organic fills. However, the **RGB** logs point to a diminishment of the organic fills towards the southern edge of the canal.

Red arrows (Fig. 8c) mark the transition from yellow-reddish to grayish sediments, indicating the assumed excavation level of the Carolingian canal. The total excavation zone is by far larger as the subsequent zone of organic fills with potential ponds. However, analogous to the direct push electrical conductivity logs the **RGB** logs also deliver indications for a lateral change in sediment facies in the lower sub-section of the cross-section (Fig. 8c: gray arrows). The gray arrows show yellowish to reddish sands at the southern edge of the cross-section that are absent within the same level at the northern edge. The lateral transition of both facies is located between 08 and 21 **RGB** logs at 410.0–411.2 m a.s.l. At this stage of investigation, we are not able to distinguish whether this change in sediment facies is naturally or probably the impact of an even deeper Carolingian excavation depth in the central part of the trench, which has been refilled by sandy colluvial material, which is very similar to the unaffected fluvial sands, but slightly colored.

Furthermore, there is also an indication for a very abrupt shift in sediment facies between 08 and 21 **RGB** log at 412.2–413.4 m a.s.l. (Fig. 8c: yellow arrow). Organic fills in 21 **RGB** log change within a

distance of only 25 cm towards grayish clastic layers in 08 RGB log. Pale coloring in 21 RGB log features evidence for wood. The abrupt shift in sediment facies might be an indication for a wooden bank stabilization within this lower zone of the organic fills.

The central zone of organic fills and the grayish colluvial deposits at the northern edge of the canal structure reveal a zone of intercalation (Fig. 8c: orange arrows between 414 and 415.5 m a.s.l.). This indicates a missing bank stabilization at that stratigraphic level.

The organic fills end with a well-preserved fen horizon (Fig. 8c: black arrow at 416.20 m a.s.l.) indicating a phase of reduced aggradation under semi-terrestrial conditions and a subsequent abrupt onset of clastic deposition. The fen horizon is ubiquitous in the central zone of the canal and the subsequent onset of clastic deposition features a distinct change in local environmental conditions.

Figs. 9b to d depict 2D visualizations for the single colorimetric proxies. We applied block kriging algorithm (size 0.5×0.5 m) constraint by geospatial correlation (variogram). The 2D visualizations show a set of homogeneous sections: I) in the lower part of the cross-section is evidence for an inclination of boundary pattern from North to South and from 415.0 to approx. 411.7 m a.s.l. The sediments below this boundary correspond with oxidized fluvial sands. These strata reveal a significant transition in green (Fig. 9c) and yellow (Fig. 9d) coloring (red arrows). II) The middle part of the cross-section reveals medium luminosity (Fig. 9b) and green (Fig. 9c, $a^* < 0$) and yellow colors (Fig. 9d, $b > 0$). This zone corresponds with reduced colluvial fills. III) In the southern part of the cross-section the colorimetric proxies indicate a homogeneous zone forming a bull-eye structure (Fig. 9b to d). This zone corresponds with the organic fills of the central zone of the canal. IV) The uppermost part of the cross-section shows medium luminosity (Fig. 9b) and red (Fig. 9c, $a^* > 0$) and yellow colors (Fig. 9d, $b^* > 0$). This zone corresponds with the upper sub-section of the driving core and electrical conductivity logs (Fig. 6a, b and f) featuring clastic sediments with varying redox conditions.

4.4. Canal cross-section: transferring sediment proxies on colorimetric data

We conduct a parameter transfer from robust KGCLT09 driving core chemical data (Fig. 6c and d) to colorimetric proxy parameters (Fig. 6h–j) and model quantitative CNS values for the entire 2D canal cross-section (Fig. 12a to d).

After depth-correction, we couple the laboratory-derived sediment data with the *in situ* direct push colorimetric logs (Fig. 9). Consequently, we are able to correlate depth-accurate colorimetric data and robust KGCLT09 sedimentological data.

To check coherence, we test linear regressions between colorimetric proxies and robust sedimentological data (Table 1, Fig. 10a to c). Additionally, we conduct a similar procedure, after running a wavelet filter algorithm (Hausmann, 2014; Hausmann et al., 2016) on CLT09 colorimetric proxies (Table 1, Fig. 10d to f). The algorithm reduces high-resolution outliers within the vertical logs.

Luminosity L^* indicates significant correlations with CNS data (Table 1, Fig. 10). In contrast, chromatographic red-green ratio a^* and blue–yellow ratio b^* reveal low coherences with CNS data. Adapting wavelet filter algorithm, we achieve higher R^2 . Exemplarily, R^2 for luminosity L^* increase for TC from 0.66 to 0.74, TN from 0.68 to 0.77, TS from 0.48 to 0.53, TOC from 0.65 to 0.73, and TOC/TN from 0.59 to 0.67 (Table 1, Fig. 10a and d).

We follow the hypothesis that multivariate regressions reveal to higher correlation. For making predictive models, we consequently apply principal component analysis on the data. Thus we achieve the colorimetric proxy luminosity L^* as component one, red-green

ratio a^* as component two, and blue-yellow ratio b^* as component three for depicting CNS data. Fig. 11 provides an example for applying of a principal component analysis on colorimetric data and on total organic carbon (TOC) from sedimentological samples (Fig. 6). As a result, TOC data are explained by luminosity L^* and red–green ratio a^* . The blue–yellow ratio slightly b^* improves the relation.

For the construction of a predictive formula, we merge the linear regression functions of the single proxies. Generally, a linear function is described by the slope equation (Eq. (1)) with y and x as the coordinates, m as the slope, and n as the y-intercept of the line. Equation (2) is the resulting predictive formula including indexed parameters from single regression. The target value y is one of the CNS data TOC, TN, TS, TC and TOC/TN. Subsequently, we fitted the single slope equation parameter m_L , m_{a^*} , m_b , and n_L from the initial stage. Stopping criteria is an achieved minimum standard deviation σ of the target value y_{mod} compared to the real measured y (Eq. (3)).

$$y = mx + n \quad (1)$$

$$y_{mod} = -m_L \cdot L^* + m_{a^*} \cdot a^* + m_b \cdot b^* + n_L \quad (2)$$

$$\sigma = \sqrt{\sum (y - y_{mod})^2}, \quad \sigma \rightarrow \min \quad (3)$$

Hence, we attain a multivariate regression model predicting TC, TN, TS, TOC, and TOC/TN on the independent colorimetric proxies luminosity L^* , red–green ratio a^* , and blue–yellow ratio b^* . However, the blue–yellow ratio b^* does not improve the regression model. Thus, b^* was rejected from the original formula (Eq. (2)). As a result, we compute multivariate regression only on the base of luminosity L^* and red–green ratio a^* . Table 2 lists parameters m and n . We achieve R^2 approx. 0.70 for TC_{mod} , TN_{mod} , TOC_{mod} , and TOC/TN_{mod} versus TC, TN, TOC, and TOC/TN, respectively. TS_{mod} versus TS shows a lower R^2 of 0.50. Adapting the similar approach on previously wavelet-filtered data, besides TS_{mod} , we generally achieve higher regression factors R^2 (Table 2).

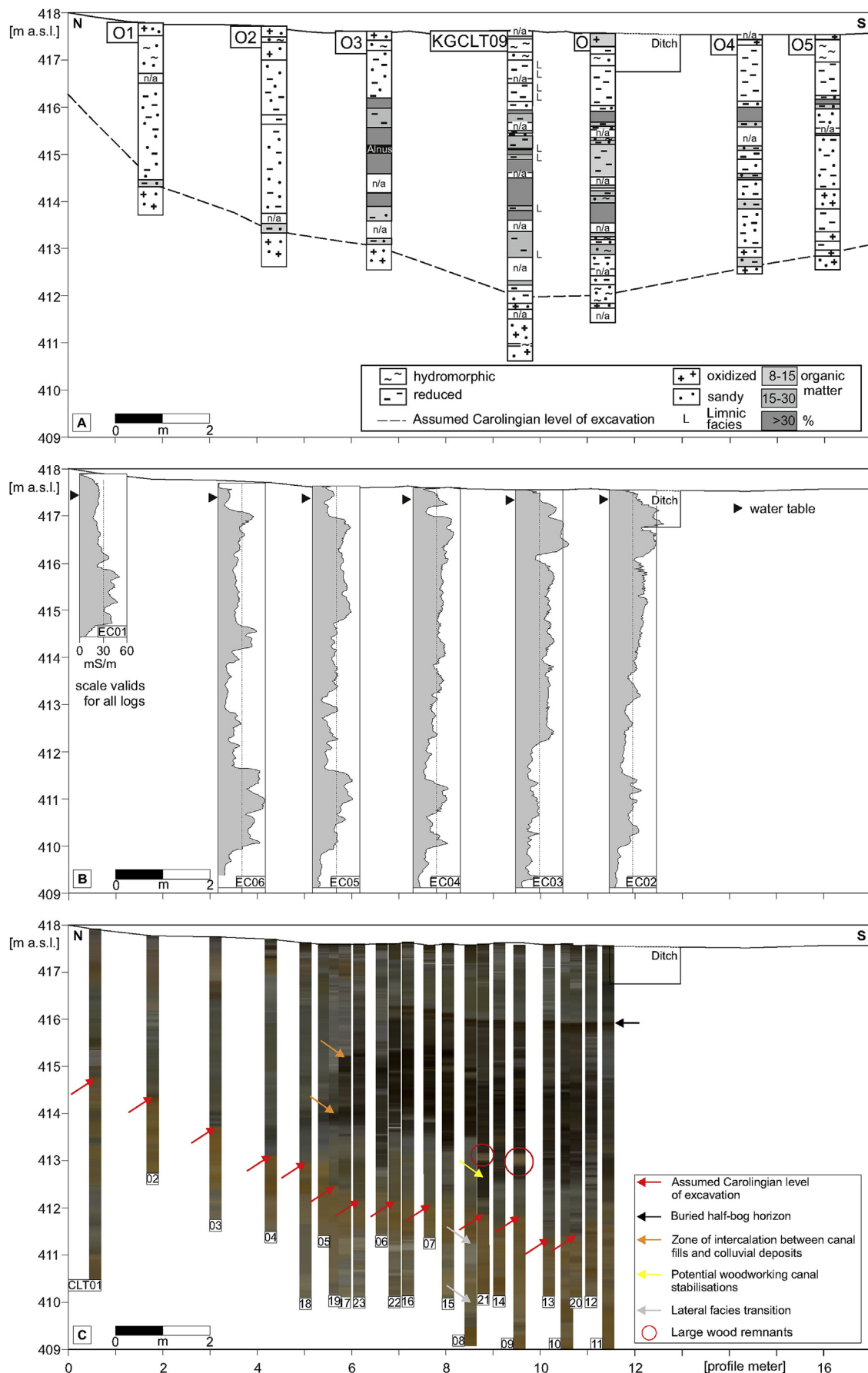
Fig. 12a to d depict a 2D visualization for predictions of TC_{mod} , TN_{mod} , TOC_{mod} , and TOC/TN_{mod} . We apply block kriging algorithm (size 0.5×0.5 m) constrained by geospatial correlation (variogram). High values of TC_{mod} , TN_{mod} , TOC_{mod} , and TOC/TN_{mod} model organic fills.

The organic-rich central zone of the canal with peat and sapropel layers is clearly visible. Furthermore, in the lowermost part the model shows higher values of TN_{mod} and TOC_{mod} at the southern edge of the cross-section between 409 and 411 m a.s.l. (Fig. 12b and c, yellow arrows), which may point to an enrichment of organic matter in the sandy material. At this stage of investigation, we are not able to distinguish whether this enrichment of organic matter is naturally or probably the impact of an even deeper Carolingian excavation depth in the central part of the trench.

5. Discussion

5.1. Direct push-derived proxy interpretation

Complementary non-invasive geophysical prospection has become an important tool in wetland geoarchaeology. Magnetic surveys (Bartington and Chapman, 2004; Linzen et al., 2009), electrical resistivity tomography (Hecht, 2009) and seismic surveys (Rabbel et al., 2004) point to varying sediment properties and layering but also archaeological anomalies. However, significant results depend on the variety of sedimentological and/or (geo)



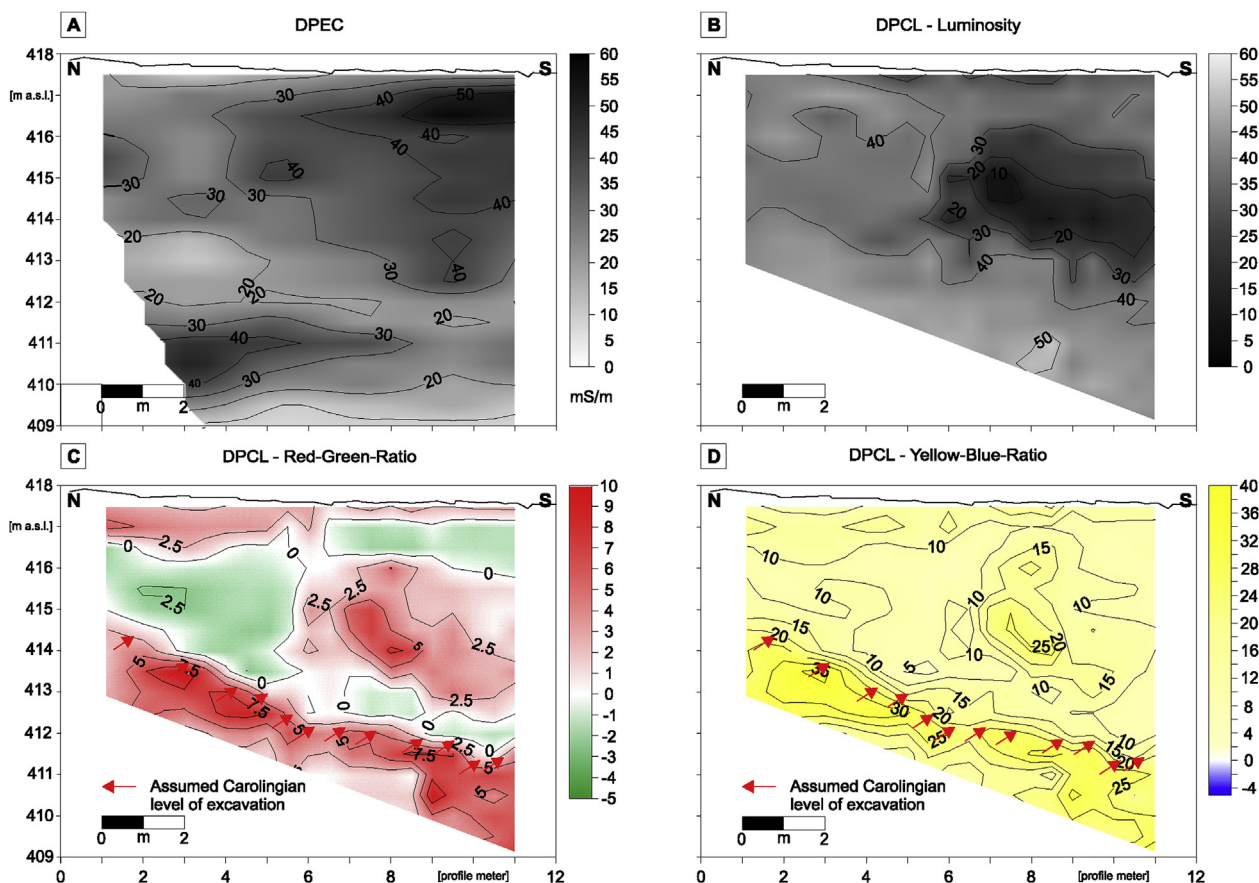


Fig. 9. 2D composite images from applied block kriging on direct push data: a) Direct push electrical conductivity (DPEC) σ (mS/m). b to d) Direct push color logging (CLT), CIEL a^* b^* color space, luminosity L^* , red-green ratio a^* , and blue-yellow ratio b^* . (For interpretation of the references to colour in this figure legend, the reader is referred to the web version of this article.)

archaeological layers but primary on their detectable geophysical differences (Lück et al., 1997; Weston, 2001; Weller and Bauerocchse, 2013). Additionally, depth-accuracies of many non-invasive geophysical prospection methods are limited and do not allow high-resolution recording at cm-scale. In this context, direct push sensing might provide an alternative tool.

Our direct push electric conductivity logs reveal a high correlation with robust grain size data from sedimentological analyses (Fig. 7 and Table 1). This is in accordance with Chouker (1971) and Schulmeister et al. (2003) who deduce high correlations between electric conductivity logs and different unconsolidated sediment textures in the saturated zone. Generally, the availability of robust sedimentological data from driving core sampling strongly improves quantitative interpretation of direct push sensing data (Dalan et al., 2011; Matney et al., 2014; Hausmann et al., 2016).

According to our results, color records might provide significant data for sediment parameterization and the detection of stratigraphic boundaries. We deduce that direct push colorimetric proxies reveal significant correlation with the total organic carbon (TOC). Eckmeier et al. (2013) have already shown that sediment darkening and increasing TOC are significantly coupled. However, these analyses bases on colorimetric measurements on dried soil samples. Regarding *in situ* color logs, it is well-known that moisture

changes influence the visible spectrum (Blavet et al., 2000; Persson, 2005; Sperling and Lazarovitch, 2010). Moisture changes, however, only influence the luminosity L^* and not the physically independent chromatographic ratios a^* (red-green) and b^* (yellow-blue) (Hausmann et al., 2016). The vertical resolution of color logs depends on the speed of sounding: the slower the pushing rate, the higher the vertical resolution of the log. The application of wavelet algorithm as a filter on the colorimetric raw data (Hausmann et al., 2016) decreases naturally color heterogeneity and lead to a higher correlation between color logs and TOC values.

5.2. Fossa Carolina: early to high medieval ponding

Within the central zone of the cross-section (Fig. 8c), between 412.5 and 416.5 m a.s.l., the RGB logs and the robust sedimentological data (middle sub-section) reveal alternating peat and sapropel layers. They represent the aquatic to semi-terrestrial zone of the canal with former ponds. According to ^{14}C dating of the organic canal fills (Zielhofer et al., 2014), major phases of sapropel accumulation and peat growing took place from the 9th to the 13th centuries. Here, ponding phases were significant during the 9th and between the 11th and 13th centuries. Hence, there is evidence that isolated zones of the West-East Section reveal open water bodies

Fig. 8. Multi-proxy compilation of the *Fossa Carolina* cross-section: a) Driving core stratigraphy with cores O to O5 (Zielhofer et al., 2014) and core KGCLT09 (this study). b) The grey shaded curves show direct push electrical conductivity (DPEC) σ (mS/m), logs EC01 to EC06, black triangles indicate the groundwater table. c) Direct push color logging (CLT) logs CLT01 to CLT23 as RGB.

Table 1

Correlation factors R^2 of linear regression between colorimetric data from **CIEL^{*} a^{*} b^{*}** color space (luminosity L^* , red-green ratio a^* , and blue-yellow ratio b^*) from direct push color logging CLT09, and CNS data for case (I) original resolution, case (II) with wavelets applied on colorimetric data, standard deviation (SD), and variance (VAR) with a total number of comparable cases N = 1177.

	TC	TN	TS	TOC	TOC/TN
<i>R² from Original resolution (I)</i>					
L^*	0.66	0.68	0.48	0.65	0.59
a^*	0.12	0.11	0.06	0.13	0.06
b^*	<0.00	<0.00	<0.00	<0.00	0.02
<i>R² from Original resolution + Wavelets (II)</i>					
L^*	0.74	0.77	0.53	0.73	0.67
a^*	0.14	0.13	0.09	0.15	0.07
b^*	<0.00	<0.00	<0.00	<0.00	0.03
<i>(I)</i>					
SD	12.77	3.30	7.78	10.64	0.51
VAR	162.95	10.90	60.60	113.30	0.26
<i>(II)</i>					
SD	12.00	2.93	6.87	10.64	0.51
VAR	144.02	8.57	47.26	113.30	0.26
	TC	TN	TS	TOC	TOC/TN

for hundreds of years. Within the Northern Section our archaeological excavation strongly supports this finding. Sapropel layers at the bottom of the canal fills indicate enduring ponding phases, which start immediately after 793 AD according to dendrochronological dating (Werther et al., 2015).

Due to the high lateral resolution of the color logs and the high depth-accuracy, a stratigraphical coupling of the single **RGB** logs is possible. As a result, we receive for the first time a clear stratigraphical evidence for an abrupt end of the aquatic to semi-terrestrial aggradation process within the central zone of the canal. The organic fills ends with a well-preserved fen horizon (Fig. 8c: black arrow at 416.20 m a.s.l.). Subsequently, an abrupt

onset of clastic deposition occurs. The high clay contents of the clastic layer (Fig. 6b) might indicate a fast accumulation of suspension load in a stillwater environment and therefore ponding as well. We assume that the clayey clastic layer represents an increase in alluvial sediment supply. This might be the result of increased water influx from the Rezat River or increased soil erosion within the Rezat headwater. According to a¹⁴C dating (1523–1619 cal AD, Zielhofer et al., 2014) the uppermost clastic layer reveals a post-Medieval age.

5.3. Fossa Carolina: abrupt Early Medieval refill of the excavated canal

At the lower part of the canal fills sandy layers with a clear fining-up (Fig. 6b) and relatively low organic contents point to an abrupt refill process. According to Zielhofer et al. (2014) there is evidence for at least 1 m of abrupt Carolingian re-deposition of sandy digging material in the West-East Section. The excavation in the Northern Section showed initial colluvial backfill processes at the edges of the canal fairway as well (Werther et al., 2015). These findings support historical sources that describe the massive refill of the canal bottom with unconsolidated bank materials after heavy rainfalls in autumn 793 AD leading to the abandonment of the Carolingian canal project (Hack, 2014). However, sapropel layers in the middle sub-section of our canal cross-section (Fig. 6a) and in the excavation further north do not confirm a definite collapse theory yet. Our findings generally indicate that the Early Medieval zone of potential ponds reveals a clearly higher position than the minimum excavation level of the Carolingian canal (Fig. 8c: red arrows). The total excavation zone is by far larger as the subsequent zone of organic fills with potential ponds.

Within the lower sub-section of the canal cross-section enhanced electrical conductivity data indicate a clayey to silty layer from approx. 409.90 to 411.70 m a.s.l. (Fig. 8b). However, these

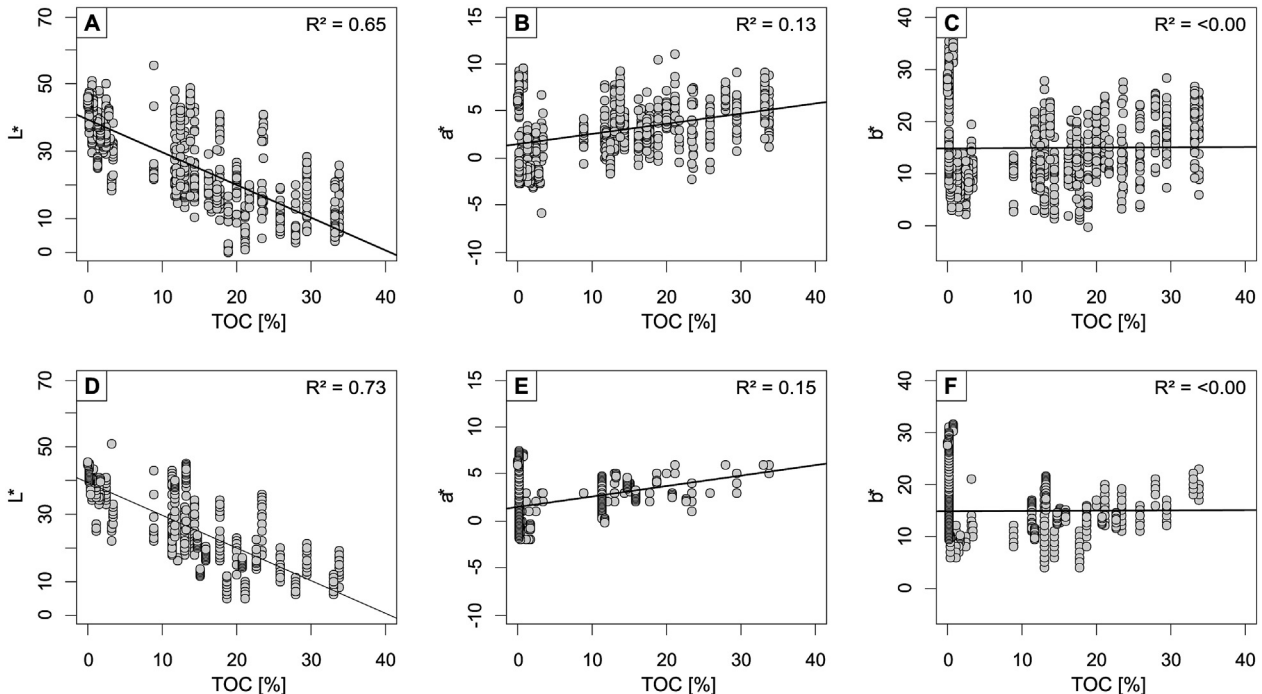


Fig. 10. Linear correlation models of total organic carbon (TOC) from CNS analysis of KGCLT09 driving core stratigraphy versus direct push color logging (CLT), log CLT09 in **CIEL^{*} a^{*} b^{*}** color space: a) and d) Luminosity L^* , b) and e) Red-green ratio a^* , c) and f) Blue-yellow ratio b^* . a–c) Original data, d–f) Applied wavelet filter for the reduction of outliers.

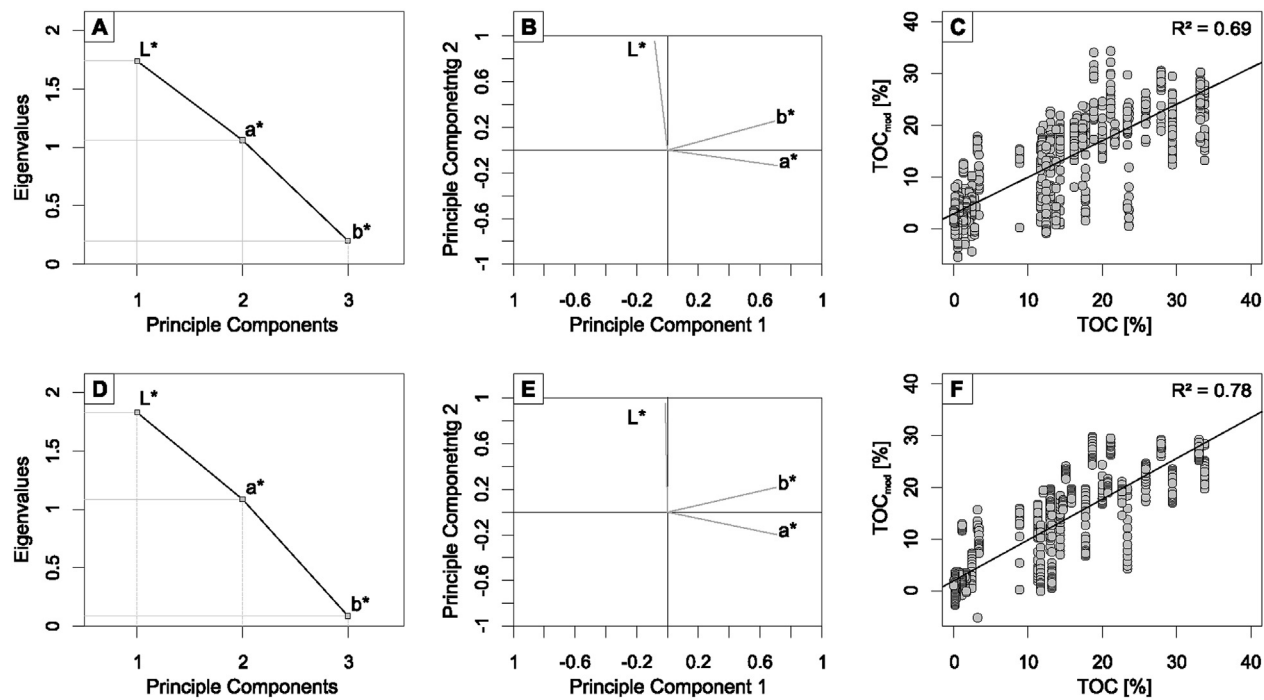


Fig. 11. Principal component analyses of colorimetric data from CIEL* a^* b^* color space (luminosity L*, red-green ratio a*, and blue-yellow ratio b*) from direct push color logging (CLT), log CLT09 versus and total organic carbon (TOC) from CNS analysis of KGCLT09 driving core stratigraphy: a) and d) Eigenvalues. b) and e) Vectorplot. c) and f) Linear correlation between measured TOC and predicted TOC_{mod}. a–c) Original data. d–f) Applied wavelet filter for reduction of outliers.

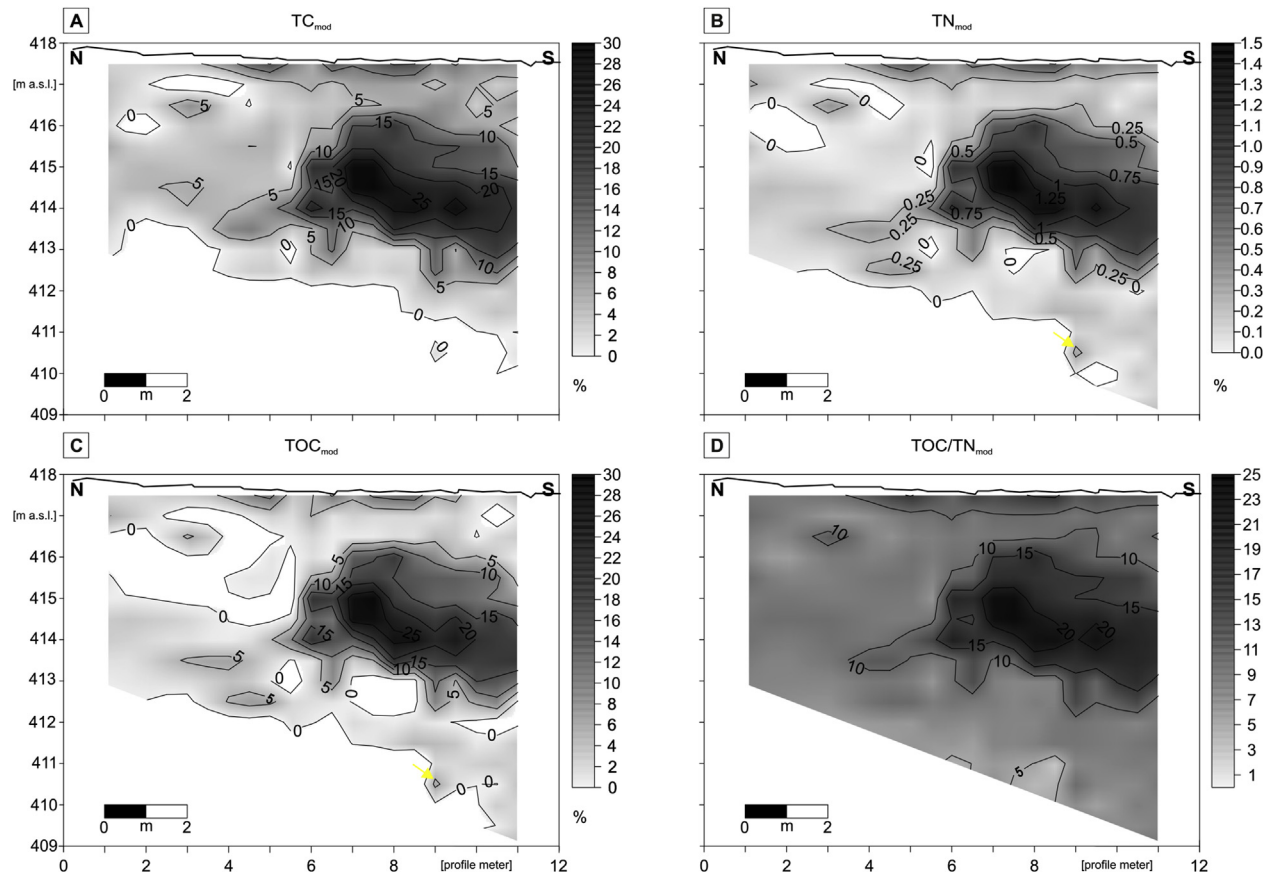


Fig. 12. 2D composite images from applied block kriging on predicted sediment parameters. a) Total carbon TC_{mod}. b) Total nitrogen TN_{mod}. c) Total organic carbon TOC_{mod}. d) TOC/TN_{mod} humidification proxy.

Table 2

Fitted parameters from stepwise regression of colorimetric data from **CIEL* a* b*** color space (luminosity L*, red-green ratio **a***, and blue-yellow ratio **b***) from direct push color logging (CLT), log CLT09 and CNS data for case (I) original resolution, case (II) with wavelets applied on color data, and correlation factors of modelled to real data (linear regression) with a total number of comparable cases N = 1177.

	Fitted parameter from stepwise regression			Modelled to real values	
	m_L^*	m_{a^*}	n_{L^*}	r	R^2
<i>Original resolution (I)</i>					
TC _{mod}	-0.64	0.63	27.53	0.83	0.70
TN _{mod}	-0.03	0.0275	1.40	0.84	0.71
TS _{mod}	-0.02	0.01	0.76	0.70	0.50
TOC _{mod}	-0.64	0.67	26.92	0.83	0.69
TOC/TN _{mod}	-0.37	0.18	23.82	0.78	0.60
<i>Original resolution + Wavelets (II)</i>					
TC _{mod}	-0.80	0.00	35.00	0.86	0.74
TN _{mod}	-0.04	0.03	1.51	0.89	0.80
TS _{mod}	-0.05	0.75	0.00	0.44	0.20
TOC _{mod}	-0.72	0.79	29.08	0.88	0.78
TOC/TN _{mod}	-0.42	0.20	25.25	0.82	0.67

enhanced electrical conductivity data are not detectable in EC03 log (Figs. 6f and 8b). The 2D visualization of interpolated electrical conductivity data similarly shows this anomaly (Fig. 9a). Analogous to the electrical conductivity logs the RGB logs also indicate a change in sediment facies at this position (Fig. 8c: gray arrows). The gray arrows show yellowish to reddish sands that are absent within the same level at the northern edge of the cross-section. The composite images of TN_{mod} and TOC_{mod} point to higher values of organic matter in this zone, too (Fig. 12a and c). At this stage of investigation, we are not able to distinguish whether this change in sediment facies is naturally or probably the impact of an even deeper Carolingian excavation level of the canal fairway, for which we had no evidence until this study. A Carolingian excavation level up to 409.5 m a.s.l. could be an interesting finding concerning the idea that the Carolingian canal was primary planned as a continuous canal and not as a summit canal. Further (geo)archaeological research is required to confirm or discard this assumption.

5.4. Fossa Carolina: indications for timber-use

Within the canal cross-section we have evidence for buried woods. This is indicated by direct push color sensing (Fig. 8c: red circle). Here, pale coloring corresponds with a recovered *Salix* wood remnant from the driving core. However, direct push color logs might indirectly reveal a probable timber-use in the West-East Section. There is evidence for a very abrupt shift in sediment facies between 21 and 08 RGB logs (Fig. 8c: yellow arrow). Organic fills in 21 RGB log change within a distance of only 25 cm towards grayish clastic layers in 08 RGB log. Such an abrupt and lateral change in sediment facies might be the result of an artificial stabilization of the Carolingian canal edge with timber. The probable use of timber is supported by recovered *Quercus* fragments within driving cores from the Central and the West East Section (Zielhofer et al., 2014). Oak remnants are not typical for a swamp forest and might indicate remnants of timber. For the Northern Section of the canal the extensive use of timber for bank stabilization is already known: an archaeological excavation recovers multiple Carolingian timber planks (Werther and Feiner, 2014; Werther et al., 2015).

The RGB logs reveal evidence for alternating phases of geomorphological activity and stagnancy that correspond with changes in organic parameters (Fig. 12a and c). The organic canal fills and the grayish colluvial deposits reveal a zone of intercalation (Fig. 8c: orange arrows between 414.0 and 415.5 m a.s.l.) indicating a missing bank stabilization at this stratigraphic level. In this zone

timber-use seems to be not in evidence.

5.5. Fossa Carolina: Early Medieval inland navigation requirements

The northern bank of the canal fairway could be located thanks to the direct push color logging between RGB log 08 and 21 (Fig. 8c: yellow arrow). For the southern bank we have no data due to a drainage ditch, which made drillings impossible. Starting from the northern bank with the assumed timber construction, the lowermost organic fill up to 412.5 m a.s.l. shows a lateral extension of at least 3.5 m, but the southern end has not been documented.

The thickness of the organic fill reaches its maximum at the deepest point of the fairway and decreases southwards and also northwards along the cross-section. This finding is supported by data from the archaeological trench in the Northern Section of the Fossa Carolina (Werther and Feiner, 2014; Werther et al., 2015) and from a driving-core derived cross-section in the North-Eastern Section (Zielhofer et al., 2014) (Fig. 2). A canal width of 3.5–5 m allows a passage of big inland vessels with a maximum width of about 3 m that corresponds with recovered Carolingian cargo scows with a payload of several tons (Ellmers and Hoffmann, 1990; Obladen-Kauder, 1994; Kröger, 2014; Zielhofer et al., 2014; Werther et al., 2015).

6. Conclusions

Robust sedimentological data from driving cores as well as colorimetric and electrical conductivity data from direct push sensing provide a 2D canal cross-section of the *Fossa Carolina* in high vertical and horizontal resolution. The data divide the cross-section in three major sub-sections: a) clastic colluvial deposits at the bottom of the Carolingian trench indicating an abrupt refill of the excavated canal during the Early Middle Ages, b) alternating sapropel and peat layers with multiple evidence for ponds during the Early Middle Ages and High Middle Ages, and finally c) clastic clay layers in the upper sub-sequence indicating a high supply of suspension load during modern times.

Direct push electric conductivity data reveal a significant correlation with grain size data. Direct push colorimetric logs provide significant correlations with total organic carbon (TOC), total nitrogen (TN), total sulphur (TS) and TOC/TN ratio. We conduct a parameter transfer from driving core-derived geochemical data to colorimetric proxy parameters and model quantitative CNS values for the entire 2D canal cross-section.

Direct push colorimetric logs reveal an abrupt shift in sediment facies within the canal cross-section that might indicate wooden bank stabilization within the Early Medieval zone of the organic canal fills. In contrast, the later intercalation of colluvial layers and organic fills in the intermediate zone of canal refills discard a potential timber-use during subsequent ponding phases.

In this study, *in situ*-obtained electrical conductivity and color logs reveal a valuable potential for distinguishing stratigraphic structures and lithological contrasts in wetland (geo)archaeology. The vertical resolution attains cm-scale. The lateral resolution is limited by the distance between the single probing positions at the surface. Here, we conduct a lateral resolution up to 25 cm. The model-based parameter transfer from robust sedimentological data and multiple one-dimensional logs toward a two-dimensional cross-section enhanced multi-proxy site information in vertical and lateral resolution.

Robust sediment data, however, are required for referencing *in situ* direct push sensing. We emphasize that a *ground truth* of direct push sensing data is generally necessary. The linkage between direct push sensing and commonly used sedimentological data from driving cores allows a significant reduction of

sedimentological sample quantities. Furthermore, continuous direct push logs strictly reduce height-inaccuracies that are commonly observed in standard driving core applications.

The cost and time effectiveness of direct push sensing, the availability of multiple geophysical probes, onsite decision-making due to direct access to the data, the high-resolution of data logs up to cm-scale, and the application range from multiple meter to multiple decameter depth provide a high potential for (geo) archaeological prospection in zones of high groundwater tables. Probable difficulties in site assessment might arise, since the application of direct push sensing in wetlands requires a sufficient ground stability that can be enhanced by using plastic boards or sand ladders.

Acknowledgments

The authors are thankful to the German Research Foundation for financial support in the scope of DFG priority program 1630 (ZI 721/10-2, ET 20/7-2) and DFG research grants (BE 5111/2-1, DI 833/19-1, ZI 721/12-1). We thank André Kirchner (now Hildesheim University), Eva Leitholdt, Katja Pöhlmann, Andreas Schneider, Birgit Schneider from Leipzig University, Peter Ettel from Friedrich Schiller University Jena, as well as Simon Kögler, Helko Kotas, Thomas Vienken and Steffen Zacharias from UFZ Helmholtz Centre for Environmental Research for multiple support during planning, technical realization and data analysis. Finally, the editors and anonymous reviewers are gratefully acknowledged for comments helping to improve the manuscript.

References

- Boden, A.G., 2005. Bodenkundliche Kartieranleitung (Pedological Mapping Guide). BGR in cooperation with German Geological Surveys, Schweizerbart, Stuttgart (in German).
- Bartington, G., Chapman, C.E., 2004. A high-stability fluxgate magnetic gradiometer for shallow geophysical survey applications. *Archaeol. Prospect.* 11, 19–34.
- Blavet, D., Mathe, E., Leprun, J.C., 2000. Relations between soil colour and water-logging duration in a representative hillside of the West African granitgneissic bedrock. *Catena* 39, 187–210.
- Brouwer, J.J.M., 2007. In-situ Soil Testing. Lankelma, East Sussex.
- Brown, A.G., 1997. Alluvial Geoarchaeology – Floodplain Archaeology and Environmental Change. Cambridge University Press, Cambridge.
- Butler, J.J., Healey, J.M., Zheng, L., McCall, W., Schulmeister, M.K., 1999. Hydrostratigraphic characterization of unconsolidated alluvial deposits with direct-push sensor technology. *Kans. Geol. Surv. Open-File Rept* 99–140.
- Chouker, F., 1971. Methodische und theoretische Untersuchungen zur geophysikalischen Grundwasseruntersuchung Freiberger Forschungshefte/C, Geophysik 271 (in German).
- Christy, C.D., Christy, T.M., Wittig, V., 1994. A percussion probing tool for direct sensing of soil conductivity. In: *Geoprobe Systems Technical Paper No. 94–100*.
- Dietrich, P., Leven, C., 2006. Direct push-technologies. In: Kirsch, J. (Ed.), *Groundwater Geophysics*. Springer, Berlin, pp. 321–340.
- Dalan, R.A., Bevan, B.W., Goodman, D., Lynch, D., De Vore, S., Adamek, S., Martin, T., Holley, G., Michlovic, M., 2011. The measurement and analysis of depth in archaeological geophysics: tests at the Biesterfeld Site, USA. *Archaeol. Prospect.* 18, 245–265.
- Doran, G.H., 2013. Excavating wet sites. In: Menotti, F., O'Sullivan, A. (Eds.), *The Oxford Handbook of Wetland Archaeology*. Oxford University Press, pp. 483–494.
- Eckmeier, E., Mavris, C., Krebs, R., Pichler, B., Egli, M., 2013. Black carbon contributes to organic matter in young soils in the Morteratsch proglacial area (Switzerland). *Biogeosciences* 10, 1265–1274.
- Ellmers, D., Hoffmann, P., 1990. Ein Frachter aus der Zeit Karls des Großen (A cargo ship of Charlemagne's era). *Bremer Archäologische Blätter N. F.* 1, 33–37 (in German).
- EPA – U.S. Environmental Protection Agency, 1997. Expedited Site Assessment Tools for Underground Storage Tank Sites: a Guideline for Regulators. USEPA Rep. 510-B-97-001. U.S. Gov. Print. Office, Pittsburgh.
- EPA – U.S. Environmental Protection Agency, 2005. Ground Water Sampling and Monitoring with Direct Push Technologies. USEPA Rep. 540/R-04/005. U.S. Gov. Print. Office, Washington.
- Ettel, P., Daim, F., Berg-Hobohm, S., Werther, L., Zielhofer, C. (Eds.), 2014. Großbaustelle 793-Das Kanalprojekt Karls des Großen zwischen Rhein und Donau (Large construction site 793 – Charlemagne's canal project between Rhine and Danube). RGZM, Mainz (in German).
- Fischer, P., Wunderlich, T., Rabbel, W., Vött, A., Willershäuser, T., Baika, K., Rigakou, D., Metallinou, G., 2016. Combined electrical resistivity tomography (ERT), direct-push electrical conductivity (DP-EC) logging and coring – a new methodological approach in geoarchaeological research. *Archaeol. Prospect.* 23 (3), 213–228.
- Gerlach, R., Fischer, P., Eckmeier, E., Hilgers, A., 2012. Buried dark soil horizons and archaeological features in the Neolithic settlement region of the Lower Rhine area, NW Germany: formation, geochemistry and chronostratigraphy. *Quat. Int.* 265, 191–204.
- Hack, A., 2014. Der Bau des Karlsgrabens nach den Schriftquellen (The construction of the Fossa Carolina – a historical review). In: Ettel, P., Daim, F., Berg-Hobohm, S., Werther, L., Zielhofer, C. (Eds.), *Großbaustelle 793 – Das Kanalprojekt Karls des Großen zwischen Rhein und Donau* (Large construction site 793 – Charlemagne's canal project between Rhine and Danube). RGZM, Mainz, pp. 53–62 (in German).
- Hartemink, A.E., Minasny, B., 2014. Towards digital soil morphometrics. *Geoderma* 230–231, 305–317.
- Hausmann, J., 2014. Parameterisation of the Near Surface by Combined Geophysical and Direct Push Techniques in the Frame of Geotechnical Site Investigation. Ph.D. Thesis. Eberhard Karls Universität Tübingen.
- Hausmann, J., Steinle, H., Kreck, M., Werban, U., Vienken, T., Dietrich, P., 2013. Two-dimensional geomorphological characterization of a filled abandoned meander using geophysical methods and soil sampling. *Geomorphology* 201, 335–343.
- Hausmann, J., Dietrich, P., Vienken, T., Werban, U., 2016. Technique, analysis routines, and application of direct push-driven in situ color logging. *Environ. Earth Sci.* 75 (11), 1–21.
- Hecht, S., 2009. Viewing the subsurface in 3D: sediment tomography for (Geo-) archaeological prospection in Palpa, southern Peru. In: Reindel, M., Wagner, G. (Eds.), *New Technologies for Archaeology*. Springer, Berlin Heidelberg, pp. 87–110.
- Hoffmann, R., Dietrich, P., 2004. An approach to determine equivalent solutions to the geoelectrical 2D inversion problem. *J. Appl. Geophys.* 56, 79–91.
- Kirchner, A., Zielhofer, C., Werther, L., Schneider, M., Linzen, S., Willken, D., Wunderlich, T., Meyer, C., Globig, P., Leitholdt, E., Berg-Hobohm, S., Ettel, P., 2017. Fossa Carolina: survey of the missing southern canal connection – an interdisciplinary approach in wetland (geo)archaeology. *Quat. Int.* in this issue.
- Koch, R., Leininger, G., 1993. Der Karlsgraben. Ergebnisse Neuer Erkundungen (Fossa Carolina – New Findings of Current Surveys), pp. 11–15. Bau intern Special Issue. Lipp, München.
- Koch, R., Kerscher, H., Küster, H., 1993. Fossa Carolina – 1200 Jahre Karlsgraben (1200-year-old Fossa Carolina). In: Denkmalpflege Informationen D 19 (In German).
- Koster, K., 2015. Cone penetration testing: a sound method for urban archaeological prospection. *Archaeol. Prospect.* 23 (19), 55–69.
- Kröger, L., 2014. Früh- und hochmittelalterliche Binnenschiffe in Mitteleuropa. Ein Überblick zum aktuellen Stand der Forschung (Early and High Medieval inland vessels in Central Europe. An overview of the current state of research). *Prahled výzkumu* 55 (2), 91–123 (in German).
- Leven, C., Weiß, H., Koschitzky, H.-P., Blum, P., Ptak, T., Dietrich, P., 2010. Direct-Push-Verfahren (Direct Push Technologies). In: *Schriftenreihe Altlastenforum Baden-Württemberg* 15. Schweizerbart'sche Verlagsbuchhandlung, Stuttgart, 36 pp (in German).
- Leven, C., Weiss, H., Vienken, T., Dietrich, P., 2011. Direct-Push-Technologien – effiziente Untersuchungsmethoden für die Untergrunderkundung (Direct Push technologies—an efficient investigation method for subsurface characterization). *Grundwasser* 16, 221–234 (in German).
- Leitholdt, E., Zielhofer, C., Berg-Hobohm, S., Schnabl, K., Kopecky-Hermanns, B., Bussmann, J., Härtling, J.W., Reicherter, K., Unger, K., 2012. Fossa Carolina: the first attempt to bridge the central european watershed—a review, new findings, and geoarchaeological challenges. *Geoarchaeology* 27, 88–104.
- Leitholdt, E., Krüger, A., Zielhofer, C., 2014. The medieval peat layer of the Fossa Carolina – evidence for bridging the central european watershed or climate control? *Z. für Geomorphol. Suppl.* 58, 189–209.
- Linzen, S., Schultz, V., Chwala, A., Schüler, T., Schulz, M., Stolz, R., Meyer, H.-G., 2009. Quantum detection meets archaeology – magnetic Prospection with SQUIDS, highly sensitive and fast. In: Reindel, M., Wagner, G. (Eds.), *New Technologies for Archaeology*. Springer, Berlin Heidelberg, pp. 71–85.
- Lunne, T., Robertson, P.K., Powell, J.J.M., 1997. Cone penetration testing in geotechnical practice. Spon Press (Taylor & Francis Group), London New York.
- Lück, E., Eisenreich, M., Spangenberg, U., Christl, G., 1997. A note on geophysical prospection of archaeological structures in urban contexts in Potsdam (Germany). *Archaeol. Prospect.* 4, 231–238.
- Matney, T., Barrett, L.R., Dawadi, M.B., Maki, D., Maxton, C., Perry, D.S., Roper, D.C., Somers, L., Whitman, L.G., 2014. In situ shallow subsurface reflectance spectroscopy of archaeological soils and features: a case-study of two Native American settlement sites in Kansas. *J. Archaeol. Sci.* 43, 315–324.
- McCall, G.W., Nielsen, D.M., Farrington, S.P., Christy, T.M., 2005. Use of direct-push technologies in environmental site characterization and ground-water monitoring. In: Nielsen, D.M. (Ed.), *Practical Handbook of Environmental Site Characterization and Ground-water*. CRS Press Taylor and Francis Group, Boca Raton, pp. 345–471.
- Menotti, F., O'Sullivan, A., 2013. *The Oxford Handbook of Wetland Archaeology*. Oxford University Press.
- Missiaen, T., Verhegge, J., Heirman, K., Crombé, P., 2015. Potential of cone penetrating testing for mapping deeply buried palaeolandscapes in the context of

- archaeological surveys in polder areas. *J. Archaeol. Sci.* 55, 174–187.
- Obladen-Kauder, J., 1994. Ein karolingischer Flusskahn aus Kalkar-Niedermörmiter (The Carolingian scow of Kalkar-Niedermörmiter). *Archäologie Im. Rheinl.* 1993, 98–99 (in German).
- Ohta, N., Robertson, A.R., 2005. Colorimetry: fundamentals and applications. In: Wiley-IS&T Series in Imaging Science and Technology, Chichester, West Sussex.
- Persson, M., 2005. Estimating surface soil moisture from soil color using image analysis. *Vadose Zone J.* 4, 1119–1122.
- Plets, R., Dix, J., Bastos, A., Best, A., 2007. Characterization of buried inundated peat on seismic (Chirp) data, inferred from core information. *Archaeol. Prospect.* 14, 261–272.
- Rabbel, W., Stuempel, H., Woelz, S., 2004. Archeological prospecting with magnetic and shear-wave surveys at the ancient city of Miletos (western Turkey). *Lead. Edge* 23, 690–703.
- Schmidt-Kaler, H., 1976. Erläuterungen zur Geologischen Karte von Bayern (Notes to the Geological Map of Bavaria) 1:25.000 (Blatt 7041 Treuchtlingen). Bayrisches Geologisches Landesamt, München (in German).
- Schmidt-Kaler, H., 1993. Geologie und Landschaftsentwicklung im Rezat-Altmühl-Bereich (geology and landscape development in Rezat-Altmühl area). Bau intern Spec. Issue. Lipp, München 8–10 (in German).
- Schulmeister, M.K., Butler, J.J., Healey, J.M., Zheng, L., Wysocki, D.A., McCall, G.W., 2003. Direct-push electrical conductivity logging for high-resolution hydrostratigraphic characterization. *Ground Water Monit. Remediat.* 23, 52–62.
- Schwarz, K., 1962. Der Main-Donau-Kanal Karls des Großen (Charlemagne's Main-Danube canal). In: Werner, J. (Ed.), Aus Bayerns Frühzeit. Friedrich Wagner Zum 75. Geburtstag. C.H. Beck'sche Verlagsbuchhandlung, München.
- Sperling, O., Lazarovitch, N., 2010. Characterization of water infiltration and redistribution for two-dimensional soil profiles by moment analyses. *Vadose Zone J.* 9, 438–444.
- Vos, P.C., Bunnik, F.P.M., Cohen, K.M., Cremer, H., 2015. A staged geogenetic approach to underwater archaeological prospection in the Port of Rotterdam (Yangtzehaven, Maasvlakte, The Netherlands): a geological and palaeoenvironmental case study for local mapping of Mesolithic lowland landscapes. *Quat. Int.* 367, 4–31.
- Werther, L., Feiner, D., 2014. Der Karlsgraben im Fokus der Archäologie. (*Fossa Carolina* – archaeological research foci). In: Ettel, P., Daim, F., Berg-Hobohm, S., Werther, L., Zielhofer, C. (Eds.), Großbaustelle 793-Das Kanalprojekt Karls des Großen zwischen Rhein und Donau (Large construction site 793 – Charlemagne's canal project between Rhine and Danube), RGZM, Mainz, pp. 33–44 (in German).
- Werther, L., Leitholdt, E., Berg-Hobohm, S., Dunkel, S., Ettel, P., Herzig, F., Kirchner, A., Linzen, S., Schneider, M., Zielhofer, C., 2015. Häfen verbinden. Neue Befunde zum Verlauf, wasserbaulichem Konzept und zur Verlandung des Karlsgrabens (Habors connect. New findings on conduct, hydroengineering concept and silting up of Fossa Carolina). In: Schmidts, T., Vucetic, M. (Eds.), Häfen im 1. Millenn. AD – Bauliche Konzepte, herrschaftliche und religiöse Einflüsse (Habors first Millenn. AD – Constr. concepts, Sover. religious Influ.). RGZM, Mainz 22, 151–185 (in German).
- Weston, D.G., 2001. Alluvium and geophysical prospection. *Archaeol. Prospect.* 8, 265–272.
- Weller, A., Bauerochse, A., 2013. Detecting organic materials in waterlogged sediments. In: Menotti, F., O'Sullivan, A. (Eds.), *The Oxford Handbook of Wetland Archaeology*. Oxford University Press, pp. 421–432.
- Wills, S.A., Burras, C.L., Sandor, J.A., 2007. Prediction of soil organic carbon content using field and laboratory measurements of soil color. *Soil Sci. Soc. Am. J.* 71, 380–388.
- Wyszecki, G., Stiles, W.S., 1982. *Color Science: Concepts and Methods, Quantitative Data and Formulae*. Wiley, New York.
- Zielhofer, C., 2004. Hydrographical and hydrochemical characteristics of karst water components (southern Franconian Jura) – a contribution to fresh water protection and karst morphogenesis. *Z. für Geomorphol. Suppl.* 136, 113–134.
- Zielhofer, C., 2009. The protection potential of soils and post-Jurassic covers against nitrate pollution in the Southern Franconian Jura, Germany. *Z. für Geomorphol.* 53, 371–386.
- Zielhofer, C., Leitholdt, E., Werther, L., Stele, A., Bussmann, J., Linzen, S., Schneider, M., Meyer, C., Berg-Hobohm, S., Ettel, P., 2014. Charlemagne's summit canal: an early medieval hydro-engineering project for passing the Central European Watershed. *PLOS ONE* 9 (9), e108194.
- Zschornack, L., Leven-Pfister, C., 2012a. Introduction to direct push technologies. In: Kästner, M., Braeckeveldt, M., Döberl, G., Cassiani, G., Papini, M.P., Leven-Pfister, C., Van Ree, D. (Eds.), *Model-driven Soil Probing, Site Assessment and Evaluation – Guidance on Technologies*. Sapienza University of Rome, Italy, pp. 149–161.
- Zschornack, L., Leven-Pfister, C., 2012b. Direct push tools for geophysical measurements. In: Kästner, M., Braeckeveldt, M., Döberl, G., Cassiani, G., Papini, M.P., Leven-Pfister, C., Van Ree, D. (Eds.), *Model-driven Soil Probing, Site Assessment and Evaluation – Guidance on Technologies*. Sapienza University of Rome, Italy, pp. 163–174.